Ecological Indicators 164 (2024) 112158

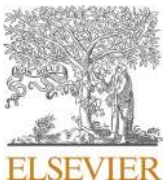

Contents lists available at ScienceDirect

Ecological Indicators

journal homepage: www.elsevier.com/locate/ecolind



Original Articles

Permafrost melting enhances growth but leads to less intra-annual density fluctuations in boreal *Larix gmelinii* forests at its southernmost limit in northeast China

Liangjun Zhu [a,b,*,1], Meng Wang [a,1], J. Julio Camarero [c], David J. Cooper [d], Danyang Yuan [e], Zecheng Chen [e], Xiaochun Wang [e,f,**], Paolo Cherubini [b,g]

[a] National Engineering Laboratory for Applied Technology of Forestry & Ecology in South China, College of Life Science and Technology, Central South University of Forestry and Technology, Changsha 410004, China
[b] Swiss Federal Institute for Forest, Snow and Landscape Research WSL, Birmensdorf, Switzerland
[c] Instituto Pirenaico de Ecología (IPE-CSIC), Avda. Montañana 1005, E-50192 Zaragoza, Spain
[d] Department of Forest and Rangeland Stewardship and Graduate Degree Program in Ecology, Colorado State University, Fort Collins, CO 80523, USA
[e] Center for Ecological Research and Key Laboratory of Sustainable Forest Ecosystem Management-Ministry of Education, School of Forestry, Northeast Forestry University, Harbin 150040, China
[f] School of Life, Qufu Normal University, Qufu, China
[g] Department of Forest and Conservation Sciences, Faculty of Forestry, University of British Columbia, 2004-2424 Main Mall, V6T 1Z4 Vancouver, BC, Canada

ARTICLE INFO

Keywords:
Tree rings
False rings
Daily climate response
Drought stress
Rapid warming
Daxing'an Mountains

ABSTRACT

Permafrost melting due to climate warming in recent decades has produced significant effects on forest ecosystems, especially the boreal biome at its southernmost limit in Asia. How this warming affects wood formation of trees at intra-annual resolution is unclear, yet is crucial for assessing the impact of permafrost melting on boreal forest growth. In this study, we compared the radial growth and intra-annual wood density fluctuations (IADFs) of Dahurian larch (*Larix gmelinii* Rupr.) at a permafrost (PF) and a non-permafrost (NPF) site at the southernmost permafrost limit in northeast China and quantified their relationships with climate factors. Drought in early summer was the main factor limiting growth of Dahurian larch. The basal area increment (BAI) of trees at both sites increased initially and then decreased in the 1980s, probably in response to warm-dry climate conditions. Earlywood IADFs (IADF-E) occurred in 14.0% and 9.3% of dated rings at the NPF and PF sites, while the frequency of latewood IADFs (IADF-L) was 6.8% and 2.7% at these two sites. The frequency of IADF-E in trees at both sites was positively and negatively related to June temperatures (and vapor pressure deficit) and precipitation, respectively, suggesting drought stress in June triggered the formation of IADF-E. The IADF-Ls were probably formed in response to warm temperatures in the late growing season. A higher BAI and a lower frequency of IADF-Es of trees at the PF site than at the NPF site indicated that permafrost melting could alleviate drought stress in early summer and promote radial growth of Dahurian larch. This greatly improved forest carbon sequestration and wood quality of some northeastern Asian boreal forests may offset to some extent the adverse effects of warming-drying climates at some sites of northeast Asia. Larch IADF-Es recorded extreme droughts in early summer, giving us a new sight for reconstructing high-frequency extreme climate events. If climate warming continues, the benefits of permafrost melting will gradually disappear and even turn negative due to warmer-dryer climate conditions. Our findings provide valuable information for boreal forest management and conservation under future global warming.

* Corresponding author at: National Engineering Laboratory for Applied Technology of Forestry & Ecology in South China, College of Life Science and Technology, Central South University of Forestry and Technology, Changsha 410004, China.
** Corresponding author at: Center for Ecological Research and Key Laboratory of Sustainable Forest Ecosystem Management-Ministry of Education, School of Forestry, Northeast Forestry University, Harbin 150040, China.
E-mail addresses: liangjun_zhu@126.com (L. Zhu), wangx@nefu.edu.cn (X. Wang).
[1] These authors contributed equally to this work.

https://doi.org/10.1016/j.ecolind.2024.112158
Received 6 February 2024; Received in revised form 29 April 2024; Accepted 18 May 2024
Available online 22 May 2024
1470-160X/© 2024 The Authors. Published by Elsevier Ltd. This is an open access article under the CC BY license (http://creativecommons.org/licenses/by/4.0/).

1. Introduction

The boreal forest accounts for approximately 30% of the global forest area, spanning the high-latitude regions of the Northern Hemisphere (FAO, 2022), and stores approximately one-third of global terrestrial carbon (Pan et al., 2011; Friedlingstein et al., 2022). Permafrost plays a crucial role in supporting the growth of almost 80% of the vegetation in boreal and hemi-boreal forests as it determines water availability and tree root development (Peng et al., 2022; Shi et al., 2024). The permafrost layer significantly diminishes hydraulic connectivity and water infiltration, and preserves soil moisture and nutrients (Jin et al., 2021). As the physical space for root growth, the active layer thickness (ALT), defined as the layer that freezes and thaws seasonally (Dobiński, 2020), also influences tree growth and forest productivity (Peng et al., 2020; Chen et al., 2022; Shi et al., 2024). However, the integrity of permafrost has been threatened by climate warming in recent decades (Wang et al., 2020; Murton, 2021). As a result of rising temperatures, the southern boundary of permafrost regions has shifted northwards by 120 km, leading to a 35% area reduction and a 25 cm increase in the average ALT (Jin et al., 2007; Carpino et al., 2018). Permafrost melting is one of the most important and dramatic manifestations of climate warming in subarctic boreal ecoregions (Carpino et al., 2018; Murton, 2021). Recent studies have shown that the interaction of permafrost melting and temperature rise has a stronger impact on forests than temperature rise alone at the southern margin of permafrost distribution (Zhang et al., 2019b; Peng et al., 2022). The permafrost melting caused by warming is related to tree growth, mainly through changes in soil stability (Li et al., 2020), water availability (Yue et al., 2020), and nutrient availability to roots (Jin et al., 2021). In the long term, permafrost melting may influence the composition, structure, and functioning of boreal and hemi-boreal forests, and should be given greater scientific attention (Peng et al., 2022). Understanding how boreal forests and different tree species cope with accelerated permafrost melting is crucial for understanding and hopefully mitigating climate change, preserving biodiversity, and maintaining the vital services provided by these ecosystems including soil carbon sequestration.

Annual rings are a valuable tool for understanding tree growth dynamics and patterns (Jing et al., 2022; Zhang et al., 2023; Zhu et al., 2023), changes in tree vitality (Cherubini et al., 2021), and reconstructing past climate variations and historical events (Zhu et al., 2021; Battipaglia et al., 2023). They have been used in studying the impact of permafrost melting on tree growth (Zhang et al., 2019a; Zhang et al., 2019b; Popkova et al., 2020; Chen et al., 2022; Peng et al., 2022). Previous studies indicated there is uncertainty about the effects of permafrost melting on tree growth in boreal regions that likely vary by species, site conditions, and permafrost types (Kirdyanov et al., 2013; Li et al., 2020; Popkova et al., 2020). It is unclear how permafrost melting affects tree xylem formation at an intra-annual scale, which is crucial for assessing the impact of climate warming or extreme weather events on tree growth and the wood quality of boreal forest trees.

Intra-annual density fluctuations (IADFs) in trees are sudden changes in wood density if the cambium activity slows down or even stops and then returns to normal growth during the early or late growing seasons (Camarero et al., 1998; Rigling et al., 2001). In conifers, IADFs appear as dark bands (latewood-like cells with small lumen and thick cell walls) of dense wood formed in the earlywood (Type IADF-E) or bright bands (earlywood-like cells with large lumen and thin cell walls) of wood with lower density formed in the latewood (Type IADF-L) (De Micco et al., 2016). IADFs in tree rings have hindered tree-ring studies because they increase the difficulty of cross-dating due to “false ring” formation. Recently, the dendrochronologist perception of IADFs have changed from “ugly duckling” to “white swan” because they can reflect how climatic extremes impact intra-annual growth (Battipaglia et al., 2016; Battipaglia et al., 2023). IADFs are considered an adjustment strategy for cambial activity to cope with favorable or unfavorable environmental conditions during the growing season. They change the structure and function of tree xylem, affecting wood quality, tree functioning, and forest productivity (Olivar et al., 2015; De Micco et al., 2016; Zalloni et al., 2016).

The formation of IADFs can be directly triggered by changes in environmental conditions. For example, the formation of IADF-E is probably related to the interruption of tracheid enlargement or division caused by climate stressors such as severe drought (Camarero et al., 2023) or late frost events (Braeuning et al., 2016) or to canopy defoliation due to biological and abiotic disturbances such as wildfire (Carroll et al., 2018) and insect outbreaks (Camarero et al., 2018). Precipitation and temperature are the climatic factors most frequently considered in relation to IADFs occurrence or their ecological role (De Micco et al., 2016; Battipaglia et al., 2023). IADFs have been widely studied in conifer species from regions exposed to seasonal drought, such as the Mediterranean Basin (Olivar et al., 2015; Pacheco et al., 2016; Camarero, 2022), North American regions (Edmondson and Jesse, 2010; Acosta-Hernández et al., 2018; Camarero, 2022), and the arid and semi-arid regions of northwest China (Zhang et al., 2020a; Gao et al., 2021a; Gao et al., 2021b; Wang et al., 2023). However, IADFs in tree rings have only been reported occasionally in boreal forests, and the impact of permafrost melting on the formation of IADFs is poorly known. This influence should be stronger near the southernmost limit of permafrost, such as in northeastern China.

The Daxing’an Mountains are a main mountain range in northeastern China, located at the southern edge of the Eurasian permafrost region. As a major driving climate factor, rapid warming since 1980s in this region has deepened permafrost active layers and led to a northward shift in the southern distribution of permafrost (Zhang et al., 2021). Permafrost in the Daxing’an Mountains can be classified into three types: extensive discontinuous, sporadic discontinuous, and isolated permafrost (Chen et al., 2020). Isolated permafrost refers to small, isolated patches or pockets of permanently frozen ground within a predominantly non-permafrost region and is highly sensitive to climate variation (Jin et al., 2007). Local topography is the main factor affecting the development of isolated permafrost. For example, permafrost is usually absent on slopes, while isolated permafrost patches occur in valleys in the central Daxing’an Mountains.

Dahurian larch (*Larix gmelinii* Rupr.), also called Gmelin larch, is native to Siberia, Mongolia, and northeastern China and is commonly found in the taiga and subarctic regions (Mamet et al., 2019). It may form pure forests in many areas and may also be mixed with *Pinus sylvestris* var. *mongolica*, *Betula platyphylla* Sukaczev and *Populus davidiana* Dode, and shrubs such as *Rhododendron dauricum* L. and *Spiraea salicifolia* L. (Zhu et al., 2018c; Chen et al., 2022). Dahurian larch is well-adapted to the harsh climate and can withstand temperatures as low as −60 °C and harsh winds. As one of the most abundant conifers in the permafrost region of Northeast Asia, it covers large areas of the mountains and contributes to the regional timber industry, habitat development, and ecosystem services. Dahurian larch has shallow roots and acquires soil water at 0–50 cm depth (Churakova-Sidorova et al., 2020). Its longevity and sensitivity of radial growth to climate warming make it an ideal species for dendrochronological analysis (Zhang et al., 2019b). Early growing season drought caused by high temperatures is the main climate factor limiting the radial growth of Dahurian larch (Peng et al., 2022). We carried out a dendrochronology study focusing on the occurrence of IADFs in Dahurian larch from the isolated permafrost areas in the Daxing’an Mountains. We focused on comparing growth in trees located on slopes without permafrost and valleys with permafrost. We hypothesized that: (1) IADFs generated in boreal forest larches correspond to the IADF-E type induced by drought stress at the beginning of the growing season; (2) larch trees in areas with permafrost (PF site) will produce fewer IADFs than trees in areas without permafrost (NPF site) due to additional water provided by the permafrost melting. By combining data on tree-ring width, basal area increment (BAI), and IADF frequency, we explored the influence of permafrost melting on wood formation in Dahurian larch.

2. Materials and methods

2.1. Study area and climate

The Daxing'an Mountains extend for about 1,200 km west to east and 400 km north to south, covering an extensive area of approximately 580,000 km^2 in northeast China (Zhu et al., 2021). This study was carried out in the central part of Daxing'an Mountains, located on the southern edge of the permafrost region in Eurasia (Fig. 1). The permafrost in the study area was recognized as the isolated permafrost (Li et al., 2008).

The region has a distinct cold temperate continental monsoonal climate, with a short, cool, wet summer and a long, cold, dry winter (Fig. 2). The growing season extends from May through September. The annual mean temperature of the study area is 3.26 °C, and July and January are the warmest (21.55 °C) and coldest (−17.09 °C) months. Total annual precipitation is 502 mm, and 73.1% of the annual precipitation occurs from June to August (Fig. 2a).

2.2. Sample collection and laboratory processing

Fieldwork was conducted in June 2017. Two larch stands without apparent human disturbance, one located on a slope (NPF: non-permafrost site) and another in the valley (PF: permafrost site), were selected at the Nanmu township in Zhalantun City of Inner Mongolia, China (Fig. 1). The two (PF and NPF) sample sites naturally formed pure Dahurian larch forests. The vast majority of larch trees in the two sites are around 50 to 60 years old, with only less than five trees in each site reaching 80 to 100 years. In order to maintain sufficient samples and avoid the potential impact of tree age, we only focused on those young

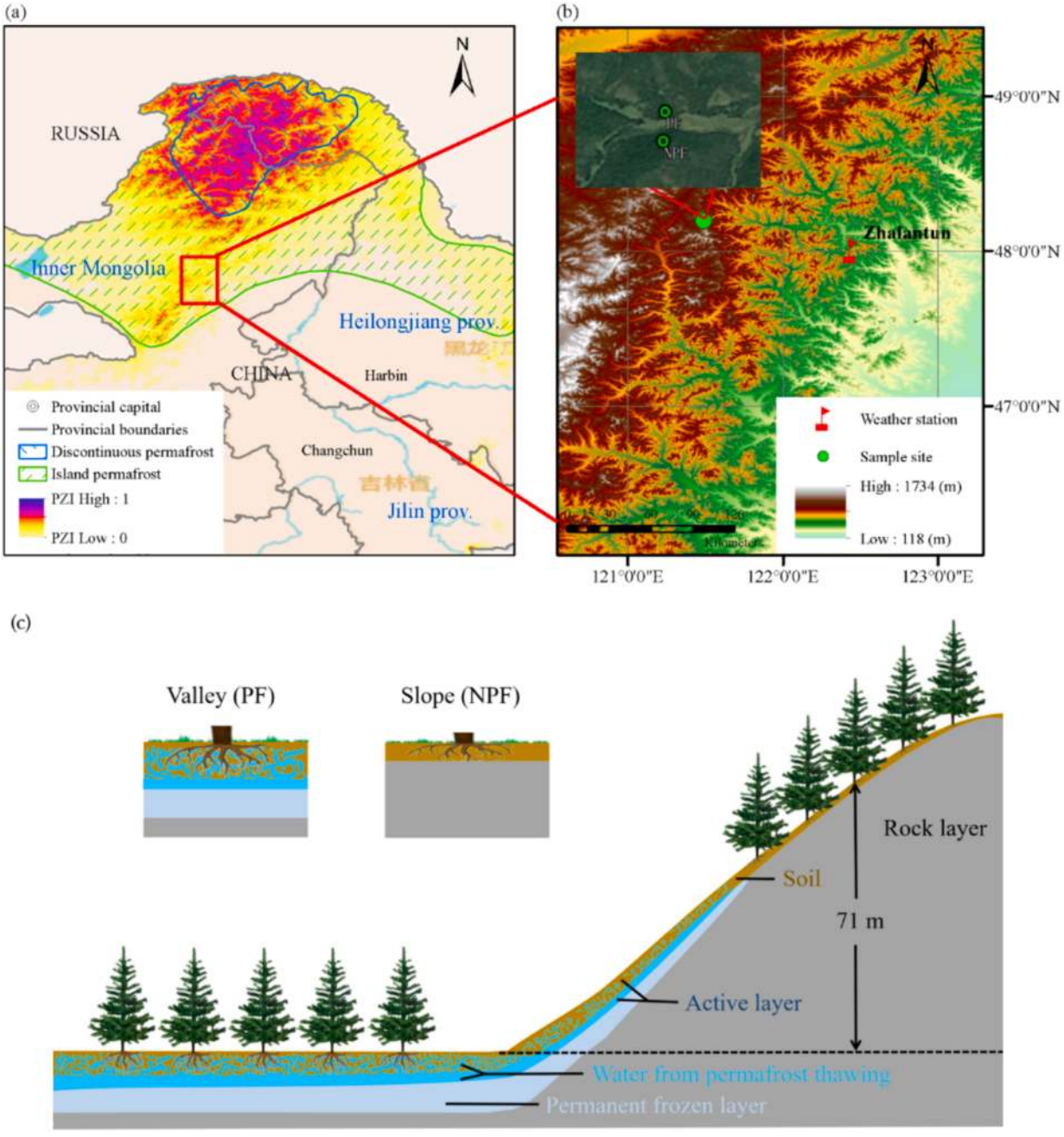

Fig. 1. (a-b) Map of the study area showing the permafrost zonation index (PZI), elevation, sample sites, and weather station. (c) Sketch map of *Larix gmelinii* sampling sites on permafrost (PF in the valley) and non-permafrost (NPF on the slope) sites.

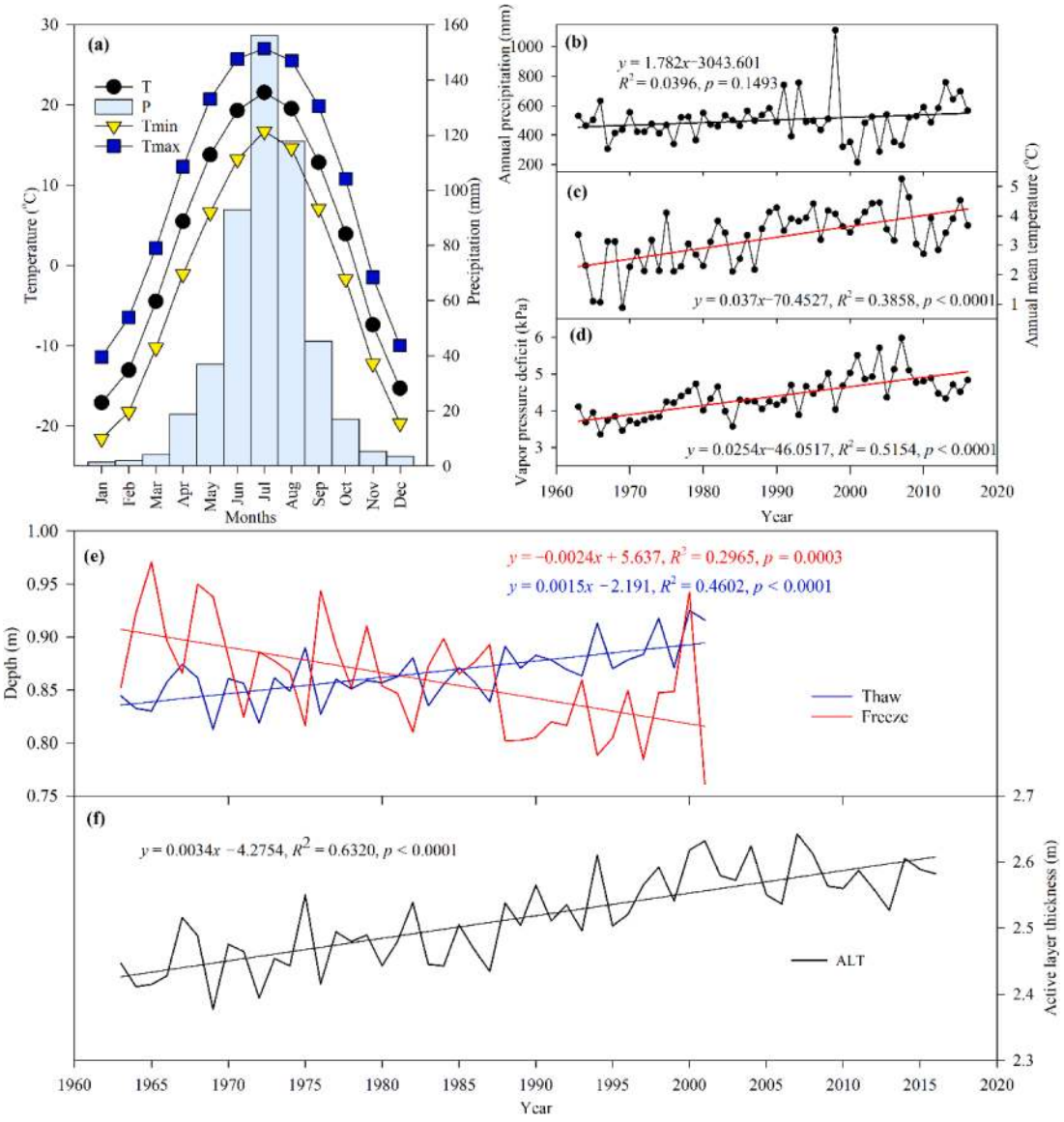

Fig. 2. (a) Climatic diagrams for the study area (Zhalantun weather station; see location in Fig. 1b). Variations in (b) precipitation, (c) mean temperature, and (d) vapor pressure deficit with fitted linear regression lines from 1963 to 2016. Annual variations with linear trends in (e) freeze and thaw depths during 1963–2001 and (f) active layer thickness (ALT) during 1963–2016 for the study area. Linear regression models, R^2, and *p*-values are listed in the plots (b-f). P = total precipitation, T = mean temperature, Tmin = minimum temperature, and Tmax = maximum temperature.

trees in this study. At each site, 20 apparently healthy dominant trees were randomly chosen for sampling. Two cores per tree were extracted at breast height (1.3 m) using a 5.15 mm diameter increment borer (Haglöf, Längsele, Sweden). Collected cores were numbered and put into plastic straws. Information on sample sites and trees was recorded, and site characteristics are in Table 1.

In the laboratory, cores were air-dried for 2–3 days and glued onto wooden sample holders. The core surface was polished with finer sandpaper progressively (240, 600, 800, and 1200 grit) until the ring boundaries and cells were clearly visible. Cores were scanned with an EPSON Expression 11000XL flatbed scanner (Seiko Epson Corporation, Japan) at 2,400 dpi resolution. Annual ring widths were measured and cross-dated with the CDendro & CooRecorder 9.5 software (Cybis Elektronik and Data AB, Sweden). The quality of tree-ring measurement was tested by cross-dating the ring-width series using the computer program COFECHA (Holmes, 1983). After removing the samples with a poor correlation to the master series, a total of 78 tree cores were used for further analysis (Table 1).

Table 1
Study species and sites where cross-dated tree-ring width chronologies of *Larix gmelinii* were developed to quantify the annual percentage of IADF production.

Site code	Latitude (°N)	Longitude (°E)	Elevation (m asl)	Topography	AGE (yrs.)	MRW ± SD (mm)	C/T	IADF proportion (%)
NPF	48.192	121.488	852	Slope	51 ± 4	0.99 ± 0.27	40/21	17.3
PF	48.195	121.487	781	Valley	52 ± 5	0.99 ± 0.28	39/20	11.3

Note: AGE is the mean tree age at 1.3 m. NPF = Non-permafrost site; PF = Permafrost site; MRW = mean ring width; C/T = No. cores/ No. trees; IADF proportion = percentage of years with intra-annual density fluctuations.

All dated raw series in this study were used to build a mean chronology of the whole series. We used the "ModNegExp" method to remove age-related trends in raw measurements. The detrended individual series were then used to calculate the ring-width chronology using a bi-weight robust mean. We finally obtained standardized ring-width chronologies for the NPF and PF sites. This process was conducted using the "dplR" package (Bunn et al., 2013) of R 4.30 statistical program (R Core Team, 2023). The tree-ring width chronologies for the NPF and PF sites are shown in Fig. 3a.

2.3. Basal area increment

Basal area increment (BAI) is increasingly used in tree-ring-based studies as it provides a direct measure of wood production and effectively accounts for growth variations or trends resulting from changes in stem circumference and size adjustments in tree growth (Zhu et al., 2018a; Jing et al., 2022). We calculated BAI from increment cores as in most previous studies by assuming ring patterns are concentric, although some bias may exist (Visser et al., 2023). In this study, most tree cores were sampled by passing to the pith, and in some cases, a few cores were not taken perpendicular to the ring borders but rather followed an arc. In situations where the pith was not included in the cores, tree age was estimated using an empirical model based on initial radial growth (Rozas, 2003). After dating to the pith, we converted the ring-width measurements into BAI values using the program BIAPlt (available at http://www.ldeo.columbia.edu/treering-laboratory/resources/software). The raw BAI of trees at the NPF and PF sites is shown in Fig. 3b.

2.4. IADF data

During visual cross-dating, we identified the occurrence of IADFs (Fig. 4) in each ring under a microscope with adequate magnification (×20–40) and a high-resolution digital microscope equipped with a LinTab™ 6.0 measuring system (Rinntech, Heidelberg, Germany). According to their relative positions, the earlywood-type (IADF-E) and latewood-type (IADF-L) density fluctuations in larch trees were identified following Campelo et al. (2007). In this study, the IADFs forming at the end stage of earlywood (IADF-E+) and latewood (IADF-L+) were not separately considered due to their extremely low frequency (Campelo et al., 2007), but they were regarded as IADF-E and IADF-L types (Fig. 4). The annual frequency (%) of IADFs is the percentage of the number of trees forming the IADF out of the total number of trees observed. IADF was counted only when both cores from the same tree showed it in the same ring (Camarero, 2022). If two types of IADFs were simultaneously exhibited in the same ring, both types were considered in this study.

2.5. Climate and permafrost data

Instrumental climate data from the Zhalantun meteorological station located near the study area (48° 00′ N, 122° 44′ E, 306.5 m a.s.l.; Fig. 1b) were obtained from the China Meteorological Information Center (http://data.cma.cn/). Daily and monthly precipitation (P), relative humidity (Rh), mean temperature (T), minimum temperature (Tmin), maximum temperature (Tmax), and extreme maximum temperature (ETmax) data from 1963 to 2016 were used in this study. Based on June ETmax, we defined extreme hot years as when years with values 1.5 times the standard deviation above the mean. According to this criterion, the years 1965, 1980, 1985, 1997, 2000, 2001, 2004, 2007, 2010, 2011, and 2014 were identified as extreme hot years.

Vapor pressure deficit (VPD) describes the difference between the amount of moisture in the air and the maximum amount of moisture the air can hold at a specific temperature (Zhong et al., 2023). It affects the movement of water vapor from the plant leaves to the surrounding air (Li et al., 2022). When VPD is high, the air is dry and can hold more moisture, causing plants to transpire more rapidly and lose water to the atmosphere. Conversely, when VPD is low, the air is already saturated

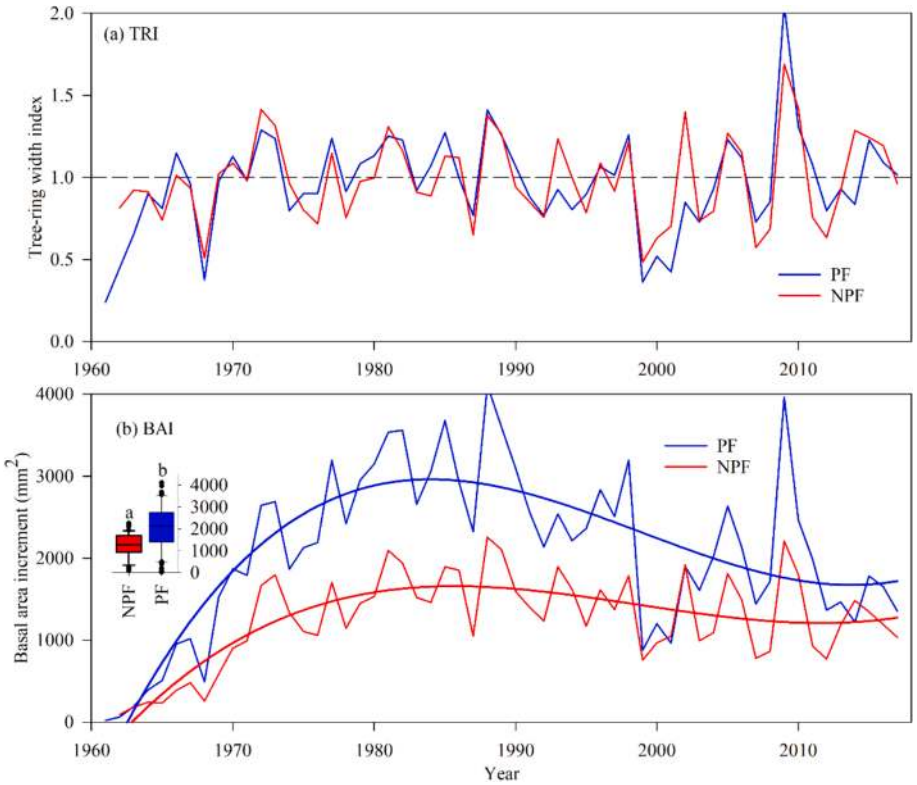

Fig. 3. (a) Mean annual tree-ring width index (TRI) and (b) annual basal area increment (BAI) of *Larix gmelinii* at the permafrost (PF) and non-permafrost (NPF) sites. Boxplot shows mean yearly BAI, and different letters indicate a significant difference in the BAI of trees at the two sites.

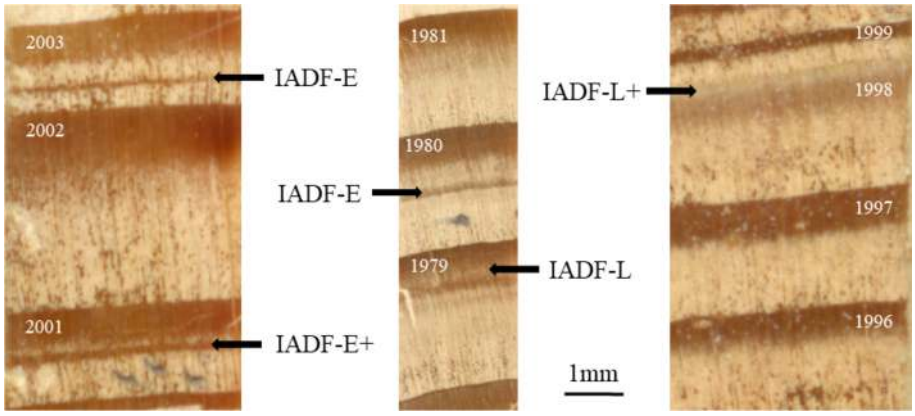

Fig. 4. Anatomical structure and relative position within a tree ring of different types of intra-annual density fluctuations (IADFs) observed in *Larix gmelinii* cores.

with moisture, and plants release less water vapor, leading to a decrease in transpiration rates (Li et al., 2022; Zhong et al., 2023). The formula used for calculating daily and monthly VPD (kPa) is:

$$VPD = 0.61078 \times e^{\frac{17.27 \times T_a}{T_a + 237.3}} \times (1 - Rh) \quad (1)$$

where T_a is the daily or monthly air temperature (^{o}C), and Rh is the daily or monthly relative humidity (%).

Long-term continuous permafrost observation data are lacking in the study area. To quantify the rate of permafrost degradation from 1963 to 2016, we estimated the ALT (m) in the valley (PF site) according to the Stefan equation. It has been extensively applied to simulate permafrost dynamics in areas with limited measurements (Wang et al., 2020; Wang and Liu, 2022; Shi et al., 2024). The simplified Stefan equation is given as:

$$ALT = E\sqrt{TI} \quad (2)$$

where E is a catchall scaling edaphic factor (E-factor) influenced by local characters including vegetation, snow cover, and local soil texture; TI is the thawing index (^{o}C day) calculated as the sum of the daily mean temperature above ^{o}C. Reference to previous research, the static site-based forest E-factor (0.046) was used to estimate ALT (Shi et al., 2024). Besides, the annual NSIDC (National Snow and Ice Data Center) freeze and thaw depths data during 1963–2001 provided by the Royal Netherlands Institute for Climate Research (https://climexp.knmi.nl) were also used to indicate changes in permafrost in recent decades.

2.6. Statistical analyses

The Shapiro-Wilk Test and Levene Test were used to check for the normality and homogeneity of the data used in this study. Linear regression was employed to examine the presence of linear temporal trends in tree growth (BAI), permafrost features, and climate variables. An independent-group *t*-test (Student's *t* test) was carried out to compare the means of annual BAI of trees at the NPF and PF sites and the means of raw ring widths of trees between the NPF and PF sites during extreme hot years. The Mann-Whitney *U* test, applicable to non-normally distributed data, was conducted to verify whether a difference in the occurrence of IADFs of trees exists at NPF and PF sites. Considering the possible impact of null values, data from years in which IADFs did not occur in trees at both PF and NPF sites were excluded before performing *U*-tests.

Spearman correlation analysis between the main monthly climate factors and the IADF frequency was used to reveal the main climate factors limiting the IADF occurrence. The daily response between the frequency of IADFs and the daily VPD was further analyzed using the *daily_response*() function in R package 'dendroTools' (Jevšenak et al., 2018). This allowed quantifying the impact of sub-monthly drought severity on IADFs occurrence and inferring the timing of IADFs development. Spearman correlation was calculated with day-wise aggregated climate data using 1,000 bootstrap samples considering all windows between 7 and 30 days from DOY 120 to 270. Correlation coefficients were calculated for the 1963–2016 period, and only those with $p < 0.05$ were used to infer the relationship between climate and IADFs. Because the tree-ring index data of trees at NPF and PF sites are normality and homogeneity, we finally performed Pearson correlation analyses to determine the main climate drivers of tree growth. Correlation coefficients between tree-ring width chronologies and climate factors from October of the previous year to September of the current year were calculated. All statistical analyses were carried out by R 4.30 (R Core Team, 2023) or SPSS13.0 (IBM, Armonk, NY, USA) software. All figures were plotted using R, Sigmaplot 14.0 (SYSTAT, San Jose, USA), or ArcMap10.8 software (ESRI, Redlands, USA).

3. Results

3.1. Trends in climate and permafrost degradation

During 1963–2016, annual mean temperatures significantly increased at +0.37 °C per decade, but no significant trend was found in total precipitation (Fig. 2b, c). Annual mean VPD also significantly increased in recent decades, indicating increasingly warmer and dryer conditions in the study area (Fig. 2d). The freeze and thaw depths significantly ($p < 0.001$) decreased and increased during 1963–2001. The ALT during 1963–2016 for the study area also significantly ($p < 0.0001$) increased at a rate of +3.4 cm per decade (Fig. 2e, f).

Temperatures (T, Tmin, and Tmax) showed significant negative correlations with freeze depths and significant positive correlations with thaw depths and ALT (Table 2). The VPD significantly positively correlated with freeze depths and negatively correlated with thaw depths and ALT, while precipitation and relative humidity had no significant correlations with these indicators of permafrost degradation (Table 2). Hence, rapid warming during 1963–2016 caused significant degradation of permafrost in the study area.

3.2. Tree growth and IADF occurrence

The BAI of PF site trees was significantly higher than that of trees at the NPF site (Fig. 3b). The BAI of trees in both NPF and PF sites increased first and then decreased around the 1980s as climate warmed and VPD rose (Figs. 1 and 3). In most extreme hot years (7 of 10), tree ring widths of trees at the PF site were significantly higher than those of trees at the NPF site (Fig. 5), indicating that permafrost melting in years with high June temperatures had a positive effect on the radial growth of Dahurian larch at the PF site compare to trees at the NPF site.

Table 2
Pearson correlation coefficients (*R*) between annual climates and three indicators of permafrost degradation.

		Thaw depths	Freeze depths	Active layer thickness (ALT)
T	*R*	0.685***	−0.736***	0.796***
	n	39	39	54
Tmin	*R*	0.664***	−0.717***	0.779***
	n	39	39	54
Tmax	*R*	0.667***	−0.669***	0.743***
	n	39	39	54
P	*R*	0.138	−0.089	0.022
	n	39	39	54
Rh	*R*	−0.056	−0.106	−0.251
	n	39	39	54
VPD	*R*	0.590***	−0.455**	0.799***
	n	39	39	54

Note: P = total precipitation, T = mean temperature, Tmin = minimum temperature, Tmax = maximum temperature, and VPD = Vapor pressure deficit. *** = $p < 0.001$ and ** = $p < 0.01$.

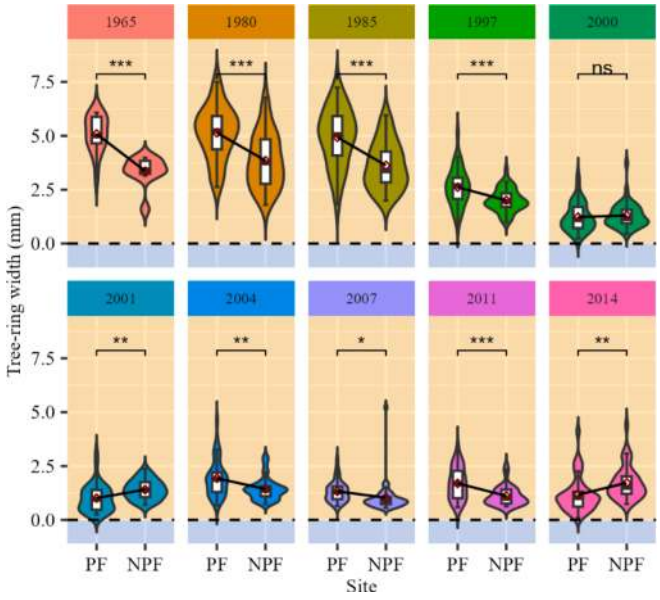

Fig. 5. Difference of raw ring widths of trees at the permafrost (PF) and non-permafrost (NPF) sites in extreme hot years. Sites with significant differences (*t*-test) were marked with stars. ns = $p > 0.05$, * = $p < 0.05$, ** = $p < 0.01$, *** = $p < 0.001$.

At both sites, the dominant IADF type in larch was the IADF-E, with 14.0% (287 rings) of total dated rings checked in the NPF site and 9.3% (180 rings) observed in the PF site (Fig. 6). IADF-L had the relatively lowest frequency with 6.8% and 2.7% (140 and 52 rings) in NPF and PF sites, respectively. Overall, the IADF frequency of the NPF site was clearly higher (not significant) than that of the PF site, whether in IADF-E, IADF-L, or the sum of the two IADF types (Fig. 6).

The number of years in which trees formed IADFs at the NPF site was also higher than at the PF site. Trees at the NPF site had nine high-frequency (exceed 0.5) IADF years (1978, 1979, 1980, 1982, 1988, 1991, 1998, 2003, and 2011), while trees at the PF site had only three years (1978, 1979, and 2011) (Fig. 6). The IADF-E and IADF-L co-occurred in five years: 1968, 1969, 1978, 1979, and 1998. In these years, the IADF frequency of the PF site was also lower than that of the NPF site (Fig. 6).

3.3. Climate drivers of IADF formation in Larix gmelinii

Spearman correlations indicated that IADF-E formation was triggered by drought at both study sites (Fig. 7). On a monthly scale, the frequency of IADF-E in larch tree rings at the two sites was positively related to June temperature (T and Tmin) and VPD, but negatively related to June precipitation. This was especially true for trees at the NPF site, which had stronger correlations than those at the PF site. The frequency of trees forming IADF-E had strong negative correlations with September mean and maximum temperatures. There were no clear relationships between the frequency of IADF-L and precipitation, temperature, and VPD (Fig. 7).

On a daily scale, the frequency of IADF-E was related to VPD from DOY 155 to DOY 175 (mid-June). The formation of IADF-E in trees at the NPF site was significantly related to VPD over a longer time range than in trees at the PF site (Fig. 8a, b). The highest correlation coefficients between IADF-E and daily VPD at the PF (0.481) and NPF (0.45) sites occurred during the same period, June 11-June 27, with an optimal window width of 17 days. The occurrence of IADF-L was positively correlated with VPD around DOY 170 (mid-June) for trees at the PF sites and negatively correlated with VPD around DOY 140 (mid-May) for trees at the NPF site (Fig. 8c, d).

Results of daily response between IADF-E and VPD showed the highest correlation coefficients occurred at the period of June 11–27 with a 17-day optimal window at both the PF and NPF (Fig. 9a, b). The relationships between IADF-E occurrence and the mean VPD of June 11–27 further showed that the probability of IADF-E occurrence significantly increased when the mean VPD of June 11–27 was greater than 9 kPa (Fig. 9c, d). The possibility of IADF-E occurrence in trees at the NPF site was higher than that at the PF site at all levels of mean VPD for the period of June 11–27 (Fig. 9c).

3.4. Climate-growth relationships

The June-July VPD showed a strong negative correlation with tree growth at the PF site, especially for June ($r = -0.315$, $p < 0.05$). Precipitation in February ($r = 0.277$, $p < 0.05$) and June ($r = 0.321$, $p < 0.05$) had positive correlations with growth at the PF site. The maximum temperature in June ($r = -0.278$, $p < 0.05$) and July ($r = -0.285$, $p < 0.05$) was negatively correlated with growth at the PF site (Fig. 10). Trees from the NPF site showed the same climate-growth relationship for these months as trees from the PF site, but were not statistically significant.

4. Discussion

4.1. Influence of climate on the formation of IADFs

The formation of IADFs can be triggered directly by changes in precipitation, temperature, and VPD that affect cambial activity and cell differentiation (De Micco et al., 2016; Battipaglia et al., 2023). In our study, the IADF-E occurred commonly at both the permafrost and non-permafrost sites, and its frequency was positively correlated with June maximum temperature and negatively correlated with June precipitation (Fig. 7). This indicates that drought conditions caused by high temperature and VPD contributed to the IADF-E formation in Dahurian larch. Daily responses further refined and clarified that the IADF-E probably occurred during June 11–27 when the mean VPD was greater than 9 kPa (Figs. 8 and 9). Drought conditions during the early growing season (mid-June) result in slow cambium activity, leading to the formation of tracheids with narrow lumen and thick walls in the earlywood (De Micco et al., 2016). Such results also coincide with other species, such as *Juniperus przewalskii* Kom. in the cold and arid environment on the northeastern Tibetan Plateau (Zhang et al., 2020a), *Pinus tabuliformis* Carrière and *Picea crassifolia* Kom. on the semi-arid Helan Mountains of north China (Gao et al., 2021b), *Pinus sylvestris* L. in the forest-steppe of southern Siberia (Arzac et al., 2021) and several conifers and broadleaf tree species in the Mediterranean region (Battipaglia et al., 2016; De Micco et al., 2016). Analyses of climate-growth

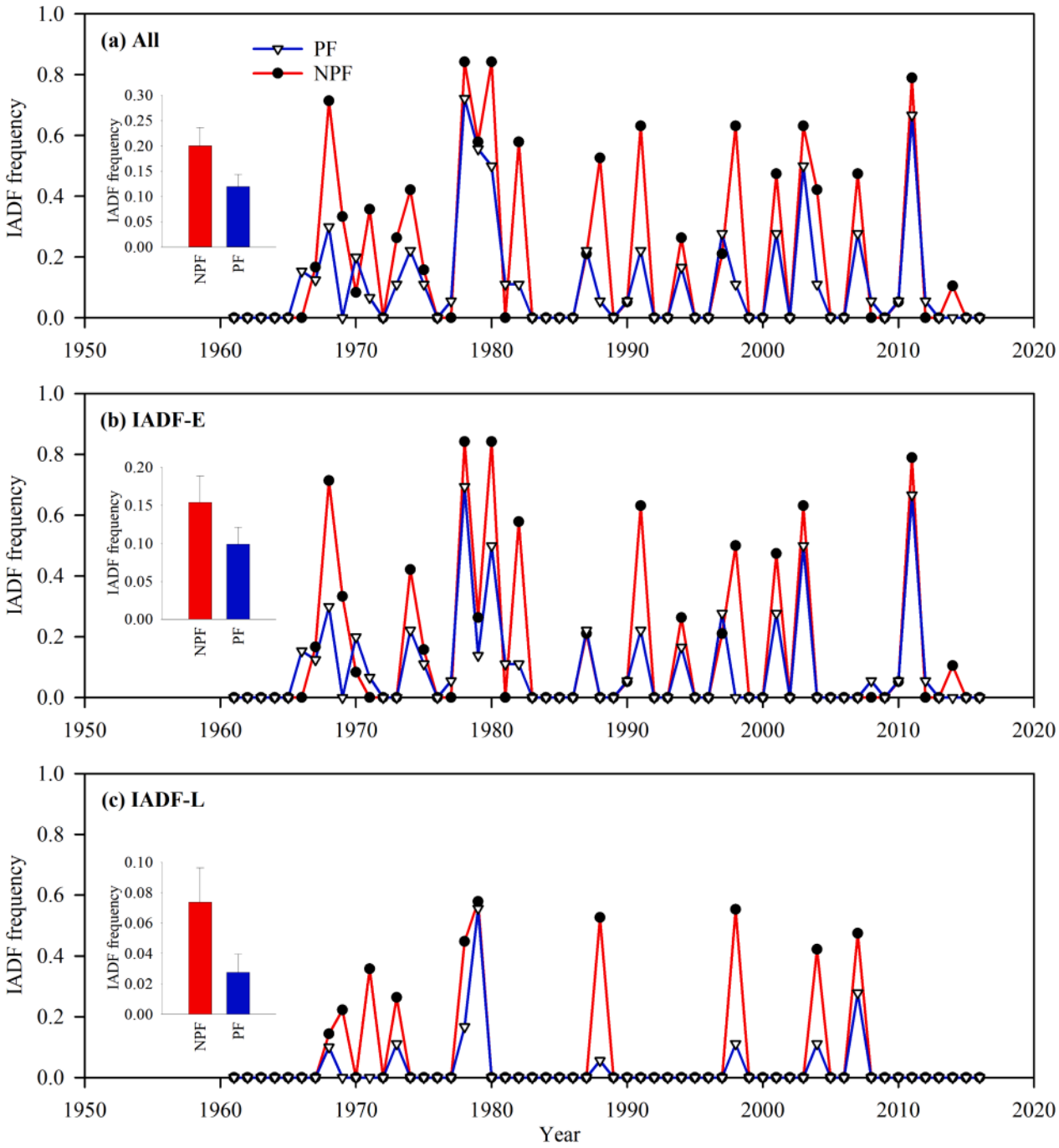

Fig. 6. Mean annual frequency of IADFs observed in the permafrost (PF) and non-permafrost (NPF) sites for the 1963–2016 period. Bar plots with error bars (standard error) show mean yearly IADF frequency.

relationships confirmed that drought in June is the main climate factor limiting the growth of Dahurian larch at both study sites (Fig. 10). This finding contrasts with most previous studies at higher latitudes or high altitudes, which found that radial growth of Dahurian larch is mainly positively influented by summer temperatures (Hellmann et al., 2016; Kharuk et al., 2023; Kirdyanov et al., 2024). However, it is in line with some studies at warmer and well-drained lower-elevation sites (Bai et al., 2019; Kirdyanov et al., 2024). This spatial variability in growth-climate relationships has been confirmed to widely exist and may be related to differences in climate and site conditions among study areas (Zhu et al., 2018b). Our results also found that the occurrence of IADF-E was negatively correlated with temperature in September. This unexpected result is likely caused by a statistically stochastic correlation since earlywood formation probably ceased by late summer.

The formation of IADF-L is a response to favorable growth conditions in late summer and early autumn, such as humid conditions or warm temperatures (De Micco et al., 2016; Camarero, 2022). In this study, however, no significant relationships were found between the IADF-L formation and climate factors (Figs. 7 and 8). Previous studies showed that warm temperatures can restore the cambial activity of trees in areas where tree cambium dormancy was mainly controlled by temperatures, such as high latitudes or high elevations (Begum et al., 2018; Zhang et al., 2020b). We found a non-significant but strong positive relationship between the IADF-L frequency and temperature in September, indicating that a warm late growing season could probably trigger the formation of IADF-L in Dahurian larch. Under warm autumn conditions,

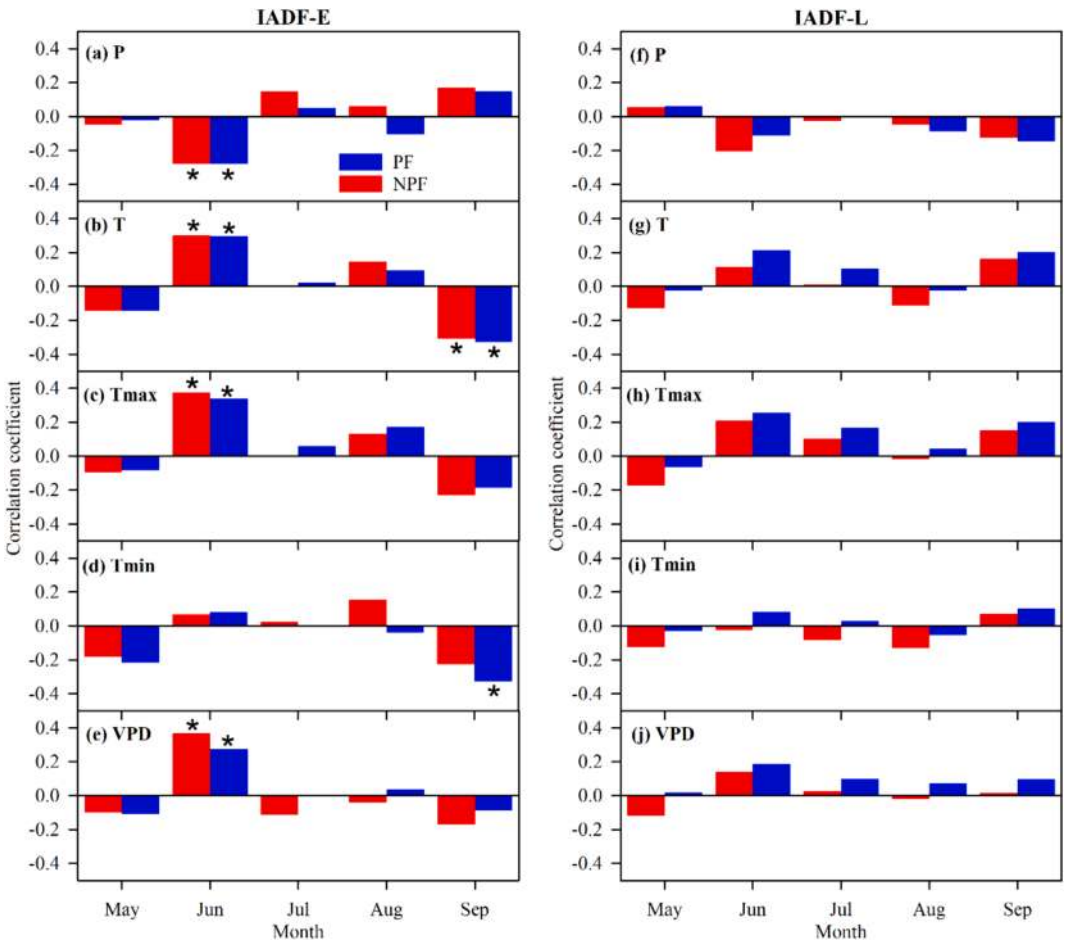

Fig. 7. Spearman correlation relationships between the frequency chronologies of IADF-E (left panel) and IADF-L (right panel) in *Larix gmelinii* at the permafrost (PF) and non-permafrost (NPF) sites and main climate factors during the period 1963–2016. Correlations were calculated only for the current growing season (May to September). Asterisks indicate $p < 0.05$. P = total precipitation, T = mean temperature, Tmin = minimum temperature, Tmax = maximum temperature, and VPD = Vapor pressure deficit.

nutrients and water stored in valley bottom soils can enhance the formation of larger tracheids, leading to IADF-L production. Besides, the formation of IADF-L could also be related to extreme weather events. For instance, the annual ring of 1998 has wide latewood with a clear "light ring" compared with other years (Fig. 4). In 1998, La Niña triggered a strong flood in China, including the Songhua River basin (Fig. 2b), which probably affected xylem dynamics and enhanced the expansion of tracheids (Pacheco et al., 2016; Peters et al., 2021). This ensures that trees have high hydraulic conductivity to cope with humid conditions. Furthermore, the occurrence of IADF-L in trees at the PF and NPF sites was positively (around DOY 170) and negatively (around DOY 140) correlated with VPD. These correlations are false and lack physiological significance since latewood probably had not yet ceased at that time (Fig. 8).

4.2. Microtopography effects on IADF frequency

From the perspective of site conditions, the types of IADFs at the two sampling sites were almost identical from year to year. Notably, the frequency of IADFs (both IADF-Es and IADF-Ls) at the NPF site was higher than at the PF site (Figs. 6 and 9), probably related to permafrost melting. The distribution of permafrost can dramatically vary across a given area (Bai et al., 2019; Li et al., 2020; Chen et al., 2022). The permafrost on slopes degrades rapidly or as even completely degraded (Ma et al., 2023), whereas the permafrost in the valley or gully degrades more slowly (Jin et al., 2007). In our study area, a permafrost layer exists in the valley PF site and thaw occurs during the beginning of the growing season (May to June). The root system of Dahurian larch is shallow, and tree roots in the valley site are close to the permafrost layer. When trees are faced with drought stress in spring, the additional water supply produced by active layer melting can alleviate drought stress to some extent and support tree growth and development (Zhang et al., 2019a; Peng et al., 2022). However, trees at the NPF site did not have this water supply to buffer drought during the early growing season.

The NPF site has lower soil water retention capacity than the PF site due to the steeper slopes, which may amplify drainage and drought conditions in the early growing season. This increases the likelihood of IADF-E formation. The results of climate-growth and climate-IADFs analyses also indicated that trees on slopes suffered more severe drought stress (Figs. 7 and 10). The internal water use efficiency of Dahurian larch at both sites has been rising steadily in recent decades and with a faster-rising rate for trees at the NPF site (Chen et al., 2022), suggesting that drought stress on the slope is more severe than in the valley. The strategy that allows tracheid formation with narrow lumen can help trees avoid xylem embolism or cavitation under drought conditions (Lauder et al., 2019). In addition, the microtopography heterogeneity leads to different growing conditions in the two sites, with better conditions in the valley (PF site) to survive harsh conditions such as long and severe droughts. These differences can explain why the frequency of IADF-E of trees growing at the PF site is significantly lower than that of trees growing at the NPF site. Similar findings and differences on growth and IADF formation have also been found in seasonally dry

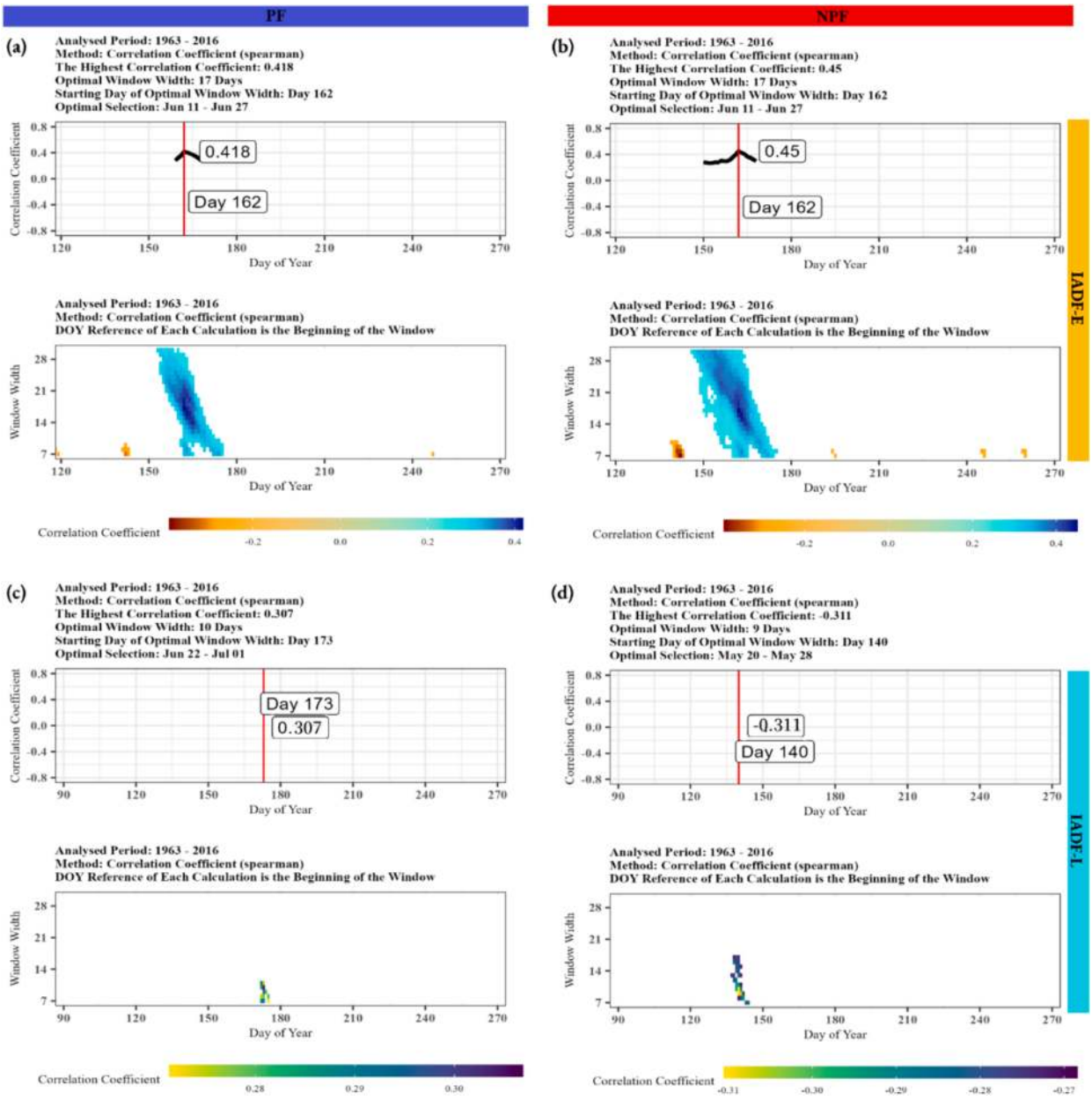

Fig. 8. Daily response (Spearman correlation) and optimal window calculated between the frequency of IADF-E (a, b) and IADF-L (c, d) in *Larix gmelinii* tree rings at the permafrost (PF) and non-permafrost (NPF) sites and the vapor pressure difference (VPD) for the 1963–2016 period. The horizontal axis represents DOY and the vertical axis represents the window size used for correlation analysis.

Mediterranean forests (Camarero et al., 2023).

4.3. Significance, implications and limitations of our study

This study demonstrates that the formation of IADFs in larch tree rings could be a good indicator of extreme climate events. This gives us new insights for reconstructing high-frequency extreme weather events in northeast China as has been done in other regions (Vieira et al., 2010). For example, the frequency of IADF-Es in larch trees has excellent potential for reconstructing extreme drought events during June at 7–10-day scales. Besides, the formation of IADFs in larch illustrates its plasticity in wood formation in response to shifts in intra-seasonal climate variations (Zalloni et al., 2016; Arzac et al., 2021). This indicates that cambium activity of Dahurian larch is highly sensitive to high-frequency climatic variations, and larches could be more robust and adaptable to sudden climate changes than species that do not form IADFs (De Micco et al., 2016). Changing wood density by regulating the division and differentiation of cambium cells in larch xylem, and forming IADFs, is a feasible, plastic, and positive response to frequent extreme climates (Camarero et al., 2014). We must admit that there is no direct evidence to determine what intensity and at what specific time drought can be reflected in wood. It may be inspired by further long-term monitoring research on the cambial dynamics of Dahurian larch and high-resolution microclimates of plots.

We found a lower frequency of IADF in trees in the permafrost area than in the areas without permafrost. This suggests that permafrost melting benefits xylem formation and radial growth of Dahurian larch (Figs. 3, 5 and 6), concurring with studies of other boreal forests (Kharuk et al., 2015; Zhang et al., 2019a; Zhang et al., 2019b). This phenomenon further supports and explains the widespread increases in vegetation cover and growth in recent decades ('greening'), especially in many cold areas located at high latitudes and high elevations in Eurasia (Myneni

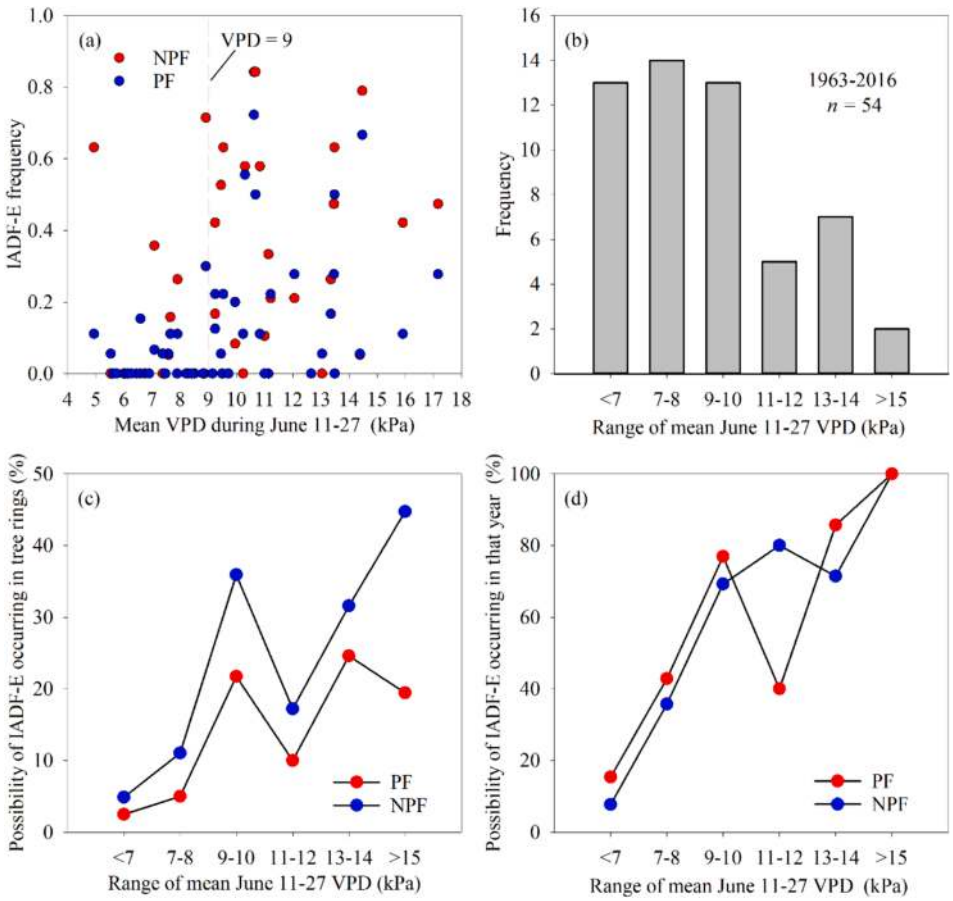

Fig. 9. Relationships between the IADF-E occurring in *Larix gmelinii* at the permafrost (PF) and non-permafrost (NPF) sites and daily vapor pressure deficit (VPD). (a) Scatter plot between mean VPD of June 11–27 and IADF-E frequency during 1963–2016. (b) Histogram of mean VPD of June 11–27 during 1963–2016. (c) Possibility of IADFs-E occurring in tree rings at different levels of mean VPD of June 11–27. (d) Possibility of IADF-Es occurring in years with different levels of mean VPD of June 11–27.

et al., 1998; Peng et al., 2020; Piao et al., 2020). Our results highlight that warming-related permafrost melting not only improves forest carbon sequestration but also preserves high wood quality (low IADFs) in the permafrost boreal biome, which may temporarily alleviate to some extent the adverse effects of warming-drying climates on forests in northeast Asia (Chang et al., 2017; Zhu et al., 2018a; Zhu et al., 2021). The differences in larch's response to climate changes provide references for forest management. For example, drought-tolerant tree species should be selected for future planting in non-permafrost regions, such as *Pinus sylvestris* var. *mongolica* Litv. and *Quercus mongolica* Fisch. ex Ledeb. (Yuan et al., 2021; Zhu et al., 2021), while deep-rooted tree species, such as *Betula platyphylla* Sukaczev, should be given priority for afforestation in permafrost areas (Peng et al., 2022). It should be emphasized that our results do not necessarily indicate that forests or trees in all regions or all species can benefit from permafrost melting (Kirdyanov et al., 2024; Shi et al., 2024). Recent studies have shown that the impact of permafrost melting on tree growth may differ among species or permafrost types (Kirdyanov et al., 2013; Li et al., 2020; Popkova et al., 2020). For example, Peng et al. (2022) found that in the isolated permafrost zone, the growth of the deep-rooted *Betula platyphylla* benefited from the water of warming-induced permafrost melting, while the shallow-rooted *Larix gmelinii* and *Larix Sibirica* Ledeb. were drought stressed. However, in the discontinuous permafrost zone, both birch and larch benefited from permafrost melting, but drought still limited larch growth (Fig. 11).

Climate models indicate that global warming will increase in the near term, and climate extremes, including heatwaves and droughts, will become more severe and frequent, especially in high-latitude areas such as northeast Asia (Zhu et al., 2021; IPCC, 2023). Under this climate scenario, it is most probable that the area with permafrost will further shrink, the permafrost will thin, and the active layer will become deeper in coming decades (Fig. 11). Trees will probably benefit from this additional water supply in the early stages of permafrost melting. However it could result in long-term severe drought for trees by accelerating water infiltration and evaporation in the future (Yue et al., 2020). These conditions would be more adverse for shallow-rooted tree species in areas with thinner permafrost layers. Therefore, the benefits of permafrost melting caused by warming will gradually disappear and even turn negative, especially for shallow-rooted tree species such as the Dahurian larch (Fig. 11) (Peng et al., 2022; Kirdyanov et al., 2024). The potential effect of permafrost melting on forest vegetation could be evaluated through the vegetation growth dynamics of aboveground parts (e.g., tree-ring width and remote-sensing data such as the Normalized Difference Vegetation Index), but permafrost melting is directly related to root system functioning rather than aboveground growth (Fig. 11). More physiological and ecological monitoring of above- and below-ground processes, combined with isotopic tracer techniques and synthetic aperture radar, could be beneficial for better understanding the mechanisms of trees responding to permafrost melt (Shi et al., 2024). Also, it is necessary to design long-term dynamic monitoring of permafrost characteristics to better understand and evaluate the relationships among climate warming, permafrost melting, and vegetation dynamics in boreal forests.

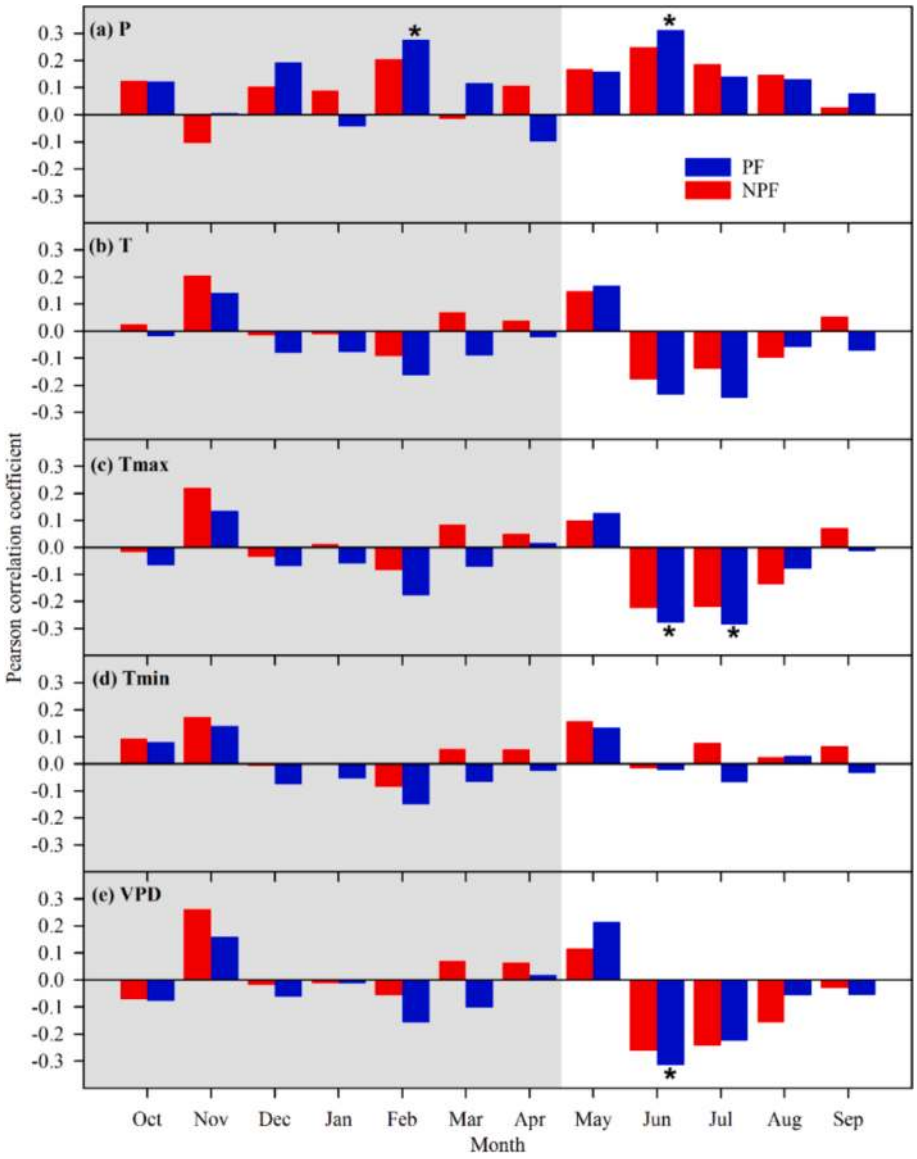

Fig. 10. Correlations (Pearson coefficient) between tree-ring width chronologies of *Larix gmelinii* at the permafrost (PF) and non-permafrost (NPF) sites and main monthly climate factors for the 1963–2016 period. Correlations were calculated from previous October to current September. The non-growing season was highlighted in the grey box. Asterisks indicate $p < 0.05$. P = total precipitation, T = mean temperature, Tmin = minimum temperature, Tmax = maximum temperature, and VPD = Vapor pressure deficit.

5. Conclusions

Drought stress caused by rapid warming in early summer was the main factor limiting the radial growth of Dahurian larch. Warm-dry climates after the 1980s led to a significant decline in growth (BAI) of trees at both the permafrost (PF) and non-permafrost (NPF) sites. At both sites, the dominant IADF-type in Dahurian larch was the IADF-E, characterized by latewood-like tracheids in the earlywood, and formed in response to dry conditions in early summer caused by low precipitation and high temperatures. The IADF-L, characterized by earlywood-like tracheids in the latewood, was rare in trees, and probably triggered by warm temperatures or extreme climate events in late summer or early autumn. Our results indicate that cambium activity of Dahurian larch was very sensitive to high-frequency climatic variability. The IADFs in larch rings could be used to reconstruct sub-monthly extreme climate events in northeastern China. Besides, the extra water supply from permafrost melting at the PF site could alleviate drought stress, resulting in a significantly higher growth (BAI or ring width) and lower frequency IADFs of trees than those at the NPF site. Our findings highlight that in its early stages warming-related permafrost melting can alleviate early summer drought stress at the PF site, resulting in an increase in larch growth and a decrease in IADF frequency. This could improve forest carbon sequestration and wood quality in the permafrost boreal forest and, to some extent, may alleviate the adverse effects of warming-drying climates at some sites in northeast Asia terrestrial ecosystems.

However, it should be emphasized that the long-term benefits of warming-related permafrost melting are limited because of differences among species and permafrost types. If climate warming continues, the benefits of permafrost melting will gradually disappear and even turn negative due to worsening in growth conditions, especially for shallow-rooted tree species such as the Dahurian larch in areas with thinner permafrost layers. Our findings also provide guidance for forest management to cope with the expected gradually worsening climatic conditions.

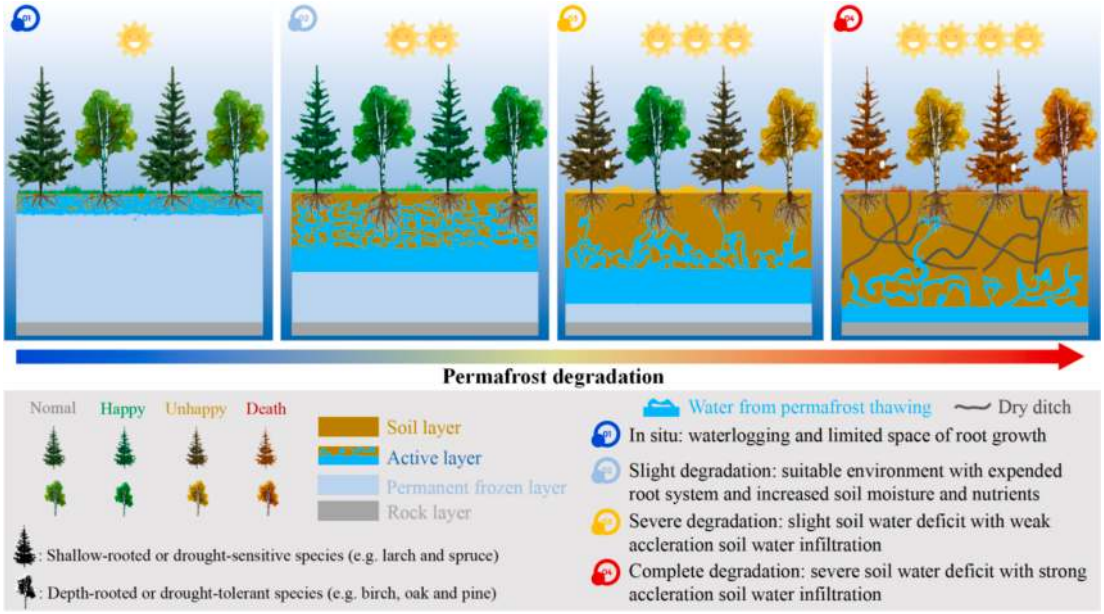

Fig. 11. Conceptual illustration of how permafrost degradation caused by rapid warming affects tree growth by changing active layers and soil environments (based on our result, Peng et al., 2022, and Shi et al., 2024).

CRediT authorship contribution statement

Liangjun Zhu: Writing – review & editing, Writing – original draft, Supervision, Methodology, Funding acquisition, Conceptualization. **Meng Wang:** Writing – original draft, Methodology, Formal analysis, Data curation. **J. Julio Camarero:** Writing – review & editing, Methodology, Conceptualization. **David J. Cooper:** Writing – review & editing, Methodology, Conceptualization. **Danyang Yuan:** Investigation, Formal analysis, Data curation. **Zecheng Chen:** Investigation, Data curation. **Xiaochun Wang:** Supervision, Funding acquisition. **Paolo Cherubini:** Writing – review & editing, Supervision, Conceptualization.

Declaration of competing interest

The authors declare that they have no known competing financial interests or personal relationships that could have appeared to influence the work reported in this paper.

Data availability

Data will be made available on request.

Acknowledgments

This research was supported by the National Natural Science Foundation of China (42107476), the Natural Science Foundation of Hunan Province (2021JJ41075), the China Postdoctoral Science Foundation (2020M682600), and the China Postdoctoral International Exchange Fellowship Program (PC2021099).

References

Acosta-Hernández, A.C., Camarero, J.J., Pompa-García, M., 2018. Seasonal growth responses to climate in wet and dry conifer forests. IAWA J. 40, 311–330.
Arzac, A., Tabakova, M.A., Khotcinskaia, K., Koteneva, A., Kirdyanov, A.V., Olano, J.M., 2021. Linking tree growth and intra-annual density fluctuations to climate in suppressed and dominant *Pinus sylvestris* L. trees in the forest-steppe of Southern Siberia. Dendrochronologia 67, 125842.
Bai, X., Zhang, X., Li, J., Duan, X., Jin, Y., Chen, Z., 2019. Altitudinal disparity in growth of Dahurian larch (*Larix gmelinii* Rupr.) in response to recent climate change in northeast China. Sci. Total Environ. 670, 466–477.
Battipaglia, G., Campelo, F., Vieira, J., Grabner, M., De Micco, V., Nabais, C., Cherubini, P., Carrer, M., Brauning, A., Cufar, K., Di Filippo, A., Garcia-Gonzalez, I., Koprowski, M., Klisz, M., Kirdyanov, A.V., Zafirov, N., de Luis, M., 2016. Structure and Function of Intra-Annual Density Fluctuations: Mind the Gaps. Front Plant Sci 7, 595.
Battipaglia, G., Kabala, J.P., Pacheco-Solana, A., Niccoli, F., Bräuning, A., Campelo, F., Cufar, K., De Luis, M., De Micco, V., Klisz, M., 2023. Intra-annual density fluctuations in tree rings are proxies of air temperature across Europe. Sci. Rep. 13, 12294.
Begum, S., Kudo, K., Rahman, M.H., Nakaba, S., Yamagishi, Y., Nabeshima, E., Nugroho, W.D., Oribe, Y., Kitin, P., Jin, H.O., Funada, R., 2018. Climate change and the regulation of wood formation in trees by temperature. Trees-Struct Funct 32, 3–15.
Braeuning, A., De Ridder, M., Zafirov, N., García-González, I., Dimitrov, D.P., Gärtner, H., 2016. Tree-ring features: indicators of extreme event impacts. IAWA J. 37, 206–231.
Bunn, A., Korpela, M., Biondi, F., Campelo, F., Zang, C., 2013. dplR: Dendrochronology Program Library in R. Dendrochronologia 26, 115–124.
Camarero, J.J., 2022. Why Intra-Annual Density Fluctuations Should Be Formed at Night? Implications for Climate-Growth Relationships in Seasonally Dry Conifer Forests. Forests 13, 1425.
Camarero, J.J., Guerrero-Campo, J., Gutierrez, E., 1998. Tree-ring growth and structure of *Pinus uncinata* and *Pinus sylvestris* in the Central Spanish Pyrenees. Arctic Alpine Res 30, 1–10.
Camarero, J.J., Rozas, V., Olano, J., 2014. Minimum wood density of *Juniperus thurifera* is a robust proxy of spring water availability in a continental Mediterranean climate. J Biogeogr 41, 1105–1114.
Camarero, J.J., Álvarez-Taboada, F., Hevia, A., Castedo-Dorado, F., 2018. Radial growth and wood density reflect the impacts and susceptibility to defoliation by gypsy moth and climate in radiata pine. Front Plant Sci 9, 1582.
Camarero, J.J., Gazol, A., Valeriano, C., Pizarro, M., González de Andrés, E., 2023. Topoclimatic modulation of growth and production of intra-annual density fluctuations in *Juniperus thurifera*. Dendrochronologia 82, 126145.
Campelo, F., Nabais, C., Freitas, H., Gutierrez, E., 2007. Climatic significance of tree-ring width and intra-annual density fluctuations in *Pinus pinea* from a dry Mediterranean area in Portugal. Ann Forest Sci 64, 229–238.
Carpino, O.A., Berg, A.A., Quinton, W.L., Adams, J.R., 2018. Climate change and permafrost thaw-induced boreal forest loss in northwestern Canada. Environ. Res. Lett. 13, 084018.
Carroll, A.L., Sillett, S.C., Van Pelt, R., 2018. Tree-ring indicators of fire in two old-growth coast redwood forests. Fire Ecology 14, 85–105.
Chang, Y., Chen, Z., Zhang, X., Bai, X., Lu, X., Zhao, X., Li, J., 2017. Responses of radial growth to temperature in *Larix gmelinii* of the Da Hinggan Ling under climate warming. Chinese Journal of Plant Ecology 41, 279–289.
Chen, S., Zang, S., Sun, L., 2020. Characteristics of permafrost degradation in Northeast China and its ecological effects: A review. Sciences in Cold and Arid Regions 12, 1–11.
Chen, Z., Zhang, Y., Li, Z., Han, S., Wang, X., 2022. Climate change increased the intrinsic water use efficiency of *Larix gmelinii* in permafrost degradation areas, but did not promote its growth. Agric. For. Meteorol. 320, 108957.
Cherubini, P., Battipaglia, G., Innes, J.L., 2021. Tree Vitality and Forest Health: Can Tree-Ring Stable Isotopes Be Used as Indicators? Curr for Rep 7, 69–80.

Churakova-Sidorova, O.V., Lienert, S., Timofeeva, G., Siegwolf, R., Saurer, M., 2020. Measured and modelled source water $\delta^{18}O$ based on tree-ring cellulose of larch and pine trees from the permafrost zone. Iforest 13, 224–229.
De Micco, V., Campelo, F., De Luis, M., Bräuning, A., Grabner, M., Battipaglia, G., Cherubini, P., 2016. Intra-annual density fluctuations in tree rings: how, when, where, and why? IAWA J. 37, 232–259.
Dobiński, W., 2020. Permafrost active layer. Earth Sci. Rev. 208, 103301.
Edmondson, Jesse, R., 2010. The Meteorological Significance of False Rings in Eastern Redcedar (*Juniperus virginiana* L.) from the Southern Great Plains, U.S.A. Tree-Ring Research 66, 19–33.
FAO, 2022. The State of the World's Forests 2022. In: FAO (Ed.), The State of the World's Forests (SOFO), Rome, Italy, pp. 1-166.
Friedlingstein, P., O'Sullivan, M., Jones, M.W., Andrew, R.M., Gregor, L., Hauck, J., Le Quéré, C., Luijkx, I.T., Olsen, A., Peters, G.P., Peters, W., Pongratz, J., Schwingshackl, C., Sitch, S., Canadell, J.G., Ciais, P., Jackson, R.B., Alin, S.R., Alkama, R., Arneth, A., Arora, V.K., Bates, N.R., Becker, M., Bellouin, N., Bittig, H.C., Bopp, L., Chevallier, F., Chini, L.P., Cronin, M., Evans, W., Falk, S., Feely, R.A., Gasser, T., Gehlen, M., Gkritzalis, T., Gloege, L., Grassi, G., Gruber, N., Gürses, Ö., Harris, I., Hefner, M., Houghton, R.A., Hurtt, G.C., Iida, Y., Ilyina, T., Jain, A.K., Jersild, A., Kadono, K., Kato, E., Kennedy, D., Klein Goldewijk, K., Knauer, J., Korsbakken, J.I., Landschützer, P., Lefèvre, N., Lindsay, K., Liu, J., Liu, Z., Marland, G., Mayot, N., McGrath, M.J., Metzl, N., Monacci, N.M., Munro, D.R., Nakaoka, S.-I., Niwa, Y., O'Brien, K., Ono, T., Palmer, P.I., Pan, N., Pierrot, D., Pocock, K., Poulter, B., Resplandy, L., Robertson, E., Rödenbeck, C., Rodriguez, C., Rosan, T.M., Schwinger, J., Séférian, R., Shutler, J.D., Skjelvan, I., Steinhoff, T., Sun, Q., Sutton, A.J., Sweeney, C., Takao, S., Tanhua, T., Tans, P.P., Tian, X., Tian, H., Tilbrook, B., Tsujino, H., Tubiello, F., van der Werf, G.R., Walker, A.P., Wanninkhof, R., Whitehead, C., Willstrand Wranne, A., Wright, R., Yuan, W., Yue, C., Yue, X., Zaehle, S., Zeng, J., Zheng, B., 2022. Global Carbon Budget 2022. Earth Syst. Sci. Data 14, 4811–4900.
Gao, J., Rossi, S., Yang, B., 2021a. Origin of intra-annual density fluctuations in a semi-arid area of northwestern China. Front Plant Sci 12, 777753.
Gao, J., Yang, B., Peng, X., Rossi, S., 2021b. Tracheid development under a drought event producing intra-annual density fluctuations in the semi-arid China. Agric. For. Meteorol. 308, 108572.
Hellmann, L., Agafonov, L., Ljungqvist, F.C., Churakova, O., Düthorn, E., Esper, J., Hülsmann, L., Kirdyanov, A.V., Moiseev, P., Myglan, V.S., Nikolaev, A.N., Reinig, F., Schweingruber, F.H., Solomina, O., Tegel, W., Büntgen, U., 2016. Diverse growth trends and climate responses across Eurasia's boreal forest. Environ. Res. Lett. 11.
Holmes, R.L., 1983. Computer-assisted quality control in tree-ring dating and measurement. Tree-Ring Bull. 43, 51–67.
IPCC, 2023. Climate Change 2023: Synthesis Report. In: Core Writing Team, H.L.a.J.R.e. (Ed.). A Report of the Intergovernmental Panel on Climate Change. Contribution of Working Groups I, II and III to the Sixth Assessment Report of the Intergovernmental Panel on Climate Change, IPCC, Geneva, Switzerland.
Jevšenak, J., Levanič, T., Džeroski, S., 2018. Comparison of an optimal regression method for climate reconstruction with the *compare_methods* function from the *dendroTools* R package. Dendrochronologia 52, 96–104.
Jin, X.-Y., Jin, H.-J., Iwahana, G., Marchenko, S.S., Luo, D.-L., Li, X.-Y., Liang, S.-H., 2021. Impacts of climate-induced permafrost degradation on vegetation: A review. Adv. Clim. Chang. Res. 12, 29–47.
Jin, H., Yu, Q., Lyu, L., Guo, D., He, R., Yu, S., Sun, G., Li, Y., 2007. Degradation of permafrost in the Xing'anling Mountains, northeastern China. Permafr. Periglac. Process. 18, 245–258.
Jing, M., Zhu, L., Liu, S., Cao, Y., Zhu, Y., Yan, W., 2022. Warming-induced drought leads to tree growth decline in subtropics: Evidence from tree rings in central China. Front Plant Sci 13, 964400.
Kharuk, V.I., Ranson, K.J., Im, S.T., Petrov, I.A., 2015. Climate-induced larch growth response within the central Siberian permafrost zone. Environ. Res. Lett. 10, 125009.
Kharuk, V.I., Petrov, I.A., Krivobokov, L.V., Golyukov, A.S., Dvinskaya, M.L., Im, S.T., Shushpanov, A.S., Smith, K.T., 2023. Larch response to warming in northern Siberia. Reg. Environ. Chang. 23.
Kirdyanov, A.V., Prokushkin, A.S., Tabakova, M.A., 2013. Tree-ring growth of Gmelin larch under contrasting local conditions in the north of Central Siberia. Dendrochronologia 31, 114–119.
Kirdyanov, A.V., Saurer, M., Arzac, A., Knorre, A.A., Prokushkin, A.S., Churakova, O.V., Arosio, T., Bebchuk, T., Siegwolf, R., Büntgen, U., 2024. Thawing permafrost can mitigate warming-induced drought stress in boreal forest trees. Science of the Total Environment 912.
Lauder, J.D., Moran, E.V., Hart, S.C., 2019. Fight or flight? Potential tradeoffs between drought defense and reproduction in conifers. Tree Physiol 39, 1071–1085.
Li, X., Cheng, G., Jin, H., Kang, E., Che, T., Jin, R., Wu, L., Nan, Z., Wang, J., Shen, Y., 2008. Cryospheric change in China. Global Planet Change 62, 210–218.
Li, Y., Liu, H., Zhu, X., Yue, Y., Xue, J., Shi, L., 2020. How permafrost degradation threatens boreal forest growth on its southern margin? Sci. Total Environ. 762, 143154.
Li, W., McDowell, N.G., Zhang, H., Wang, W., Mackay, D.S., Leff, R., Zhang, P., Ward, N. D., Norwood, M., Yabusaki, S., Myers-Pigg, A.N., Pennington, S.C., Pivovaroff, A.L., Waichler, S., Xu, C., Bond-Lamberty, B., Bailey, V.L., 2022. The influence of increasing atmospheric CO2, temperature, and vapor pressure deficit on seawater-induced tree mortality. New Phytol. 235, 1767–1779.
Ma, M., Chen, H., Ma, Y., 2023. Numerical evaluation of thermal stability of a W-shaped crushed-rock embankment with shady and sunny slopes in warm permafrost regions. Int. Commun. Heat Mass Transfer 144, 106754.
Mamet, S.D., Brown, C.D., Trant, A.J., Laroque, C.P., 2019. Shifting global *Larix* distributions: Northern expansion and southern retraction as species respond to changing climate. J Biogeogr 46, 30–44.
Murton, J.B., 2021. Permafrost and climate change. In: Letcher, T.M. (Ed.), Climate Change (third Edition). Elsevier, pp. 281–326.
Myneni, R., Tucker, C., Asrar, G., Keeling, C., 1998. Interannual variations in satellite-sensed vegetation index data from 1981 to 1991. J Geophys Res-Atmos 103, 6145–6160.
Olivar, J., Rathgeber, C., Bravo, F., 2015. Climate change, tree-ring width and wood density of pines in mediterranean environments. IAWA J. 36, 257–269.
Pacheco, A., Camarero, J.J., Carrer, M., 2016. Linking wood anatomy and xylogenesis allows pinpointing of climate and drought influences on growth of coexisting conifers in continental Mediterranean climate. Tree Physiol 36, 502–512.
Pan, Y., Birdsey, R.A., Fang, J., Houghton, R., Kauppi, P.E., Kurz, W.A., Phillips, O.L., Shvidenko, A., Lewis, S.L., Canadell, J.G., Ciais, P., Jackson, R.B., Pacala, S.W., McGuire, A.D., Piao, S., Rautiainen, A., Sitch, S., Hayes, D., 2011. A large and persistent carbon sink in the world's forests. Science 333, 988–993.
Peng, R., Liu, H., Anenkhonov, O.A., Sandanov, D.V., Korolyuk, A.Y., Shi, L., Xu, C., Dai, J., Wang, L., 2022. Tree growth is connected with distribution and warming-induced degradation of permafrost in southern Siberia. Glob. Chang. Biol. 28, 5243–5253.
Peng, X., Zhang, T., Frauenfeld, O.W., Wang, S., Qiao, L., Du, R., Mu, C., 2020. Northern hemisphere greening in association with warming permafrost. J Geophys Res-Biogeo 125, e2019JG005086.
Peters, R.L., Steppe, K., Cuny, H.E., De Pauw, D.J.W., Frank, D.C., Schaub, M., Rathgeber, C.B.K., Cabon, A., Fonti, P., 2021. Turgor-a limiting factor for radial growth in mature conifers along an elevational gradient. New Phytol. 229, 213–229.
Piao, S.L., Wang, X.H., Park, T., Chen, C., Lian, X., He, Y., Bjerke, J.W., Chen, A.P., Ciais, P., Tommervik, H., Nemani, R.R., Myneni, R.B., 2020. Characteristics, drivers and feedbacks of global greening. Nat Rev Earth Env 1, 14–27.
Popkova, M.I., Shishov, V.V., Vaganov, E.A., Fonti, M.V., Kirdyanov, A.V., Babushkina, E. A., Huang, J.G., Rossi, S., 2020. Contribution of Xylem Anatomy to Tree-Ring Width of Two Larch Species in Permafrost and Non-Permafrost Zones of Siberia. Forests 11, 1343.
R Core Team, R., 2023. R: A language and environment for statistical computing. In. R Foundation for Statistical Computing, Vienna, Austria.
Rigling, A., Waldner, P.O., Forster, T., BraSker, O.U., Pouttu, A., 2001. Ecological interpretation of tree-ring width and intraannual density fluctuations in *Pinus sylvestris* on dry sites in the central Alps and Siberia. Can J Forest Res 31, 18–31.
Rozas, V., 2003. Tree age estimates in *Fagus sylvatica* and *Quercus robur*: testing previous and improved methods. Plant Ecol 167, 193–212.
Shi, L., Liu, H., Wang, L., Peng, R., He, H., Liang, B., Cao, J., 2024. Transitional responses of tree growth to climate warming at the southernmost margin of high latitudinal permafrost distribution. Sci. Total Environ. 908, 168503.
Vieira, J., Campelo, F., Nabais, C., 2010. Intra-annual density fluctuations of Pinus pinaster are a record of climatic changes in the western Mediterranean region. Can J Forest Res 40, 1567–1575.
Visser, H., van der Maaten-Theunissen, M., van der Maaten, E., 2023. BAI BAI bias–An evaluation of uncertainties in calculating basal area increments from cores. Dendrochronologia 78, 126066.
Wang, S., Deng, Y., Gao, L., Zhang, Y., Shi, X., Gou, X., 2023. Influence of monsoon anomalies on intra-annual density fluctuations of Chinese pine in the Loess Plateau. Int J Biometeorol 67, 847–856.
Wang, J., Liu, D.S., 2022. Vegetation green-up date is more sensitive to permafrost degradation than climate change in spring across the northern permafrost region. Glob. Chang. Biol. 28, 1569–1582.
Wang, T., Yang, D., Yang, Y., Piao, S., Li, X., Cheng, G., Fu, B., 2020. Permafrost thawing puts the frozen carbon at risk over the Tibetan Plateau. Sci. Adv. 6, eaaz3513.
Yuan, D., Zhu, L., Cherubini, P., Li, Z., Zhang, Y., Wang, X., 2021. Species-specific indication of 13 tree species growth on climate warming in temperate forest community of northeast China. Ecol Indic 133, 108389.
Yue, Y., Liu, H., Xue, J., Li, Y., Guo, W., 2020. Ecological indicators of near-surface permafrost habitat at the southern margin of the boreal forest in China. Ecol Indic 108, 105714.
Zalloni, E., de Luis, M., Campelo, F., Novak, K., De Micco, V., Di Filippo, A., Vieira, J., Nabais, C., Rozas, V., Battipaglia, G., 2016. Climatic signals from intra-annual density fluctuation frequency in mediterranean pines at a regional scale. Front Plant Sci 7, 579.
Zhang, J., Alexander, M.R., Gou, X., Deslauriers, A., Pederson, N., 2020a. Extended xylogenesis and stem biomass production in *Juniperus przewalskii* Kom. during extreme late-season climatic events. Ann Forest Sci 77, 1–11.
Zhang, X., Bai, X., Hou, M., Chen, Z., Manzanedo, R.D., 2019a. Warmer winter ground temperatures trigger rapid growth of dahurian larch in the permafrost forests of northeast China. J Geophys Res-Biogeo 124, 1088–1097.
Zhang, S., Belien, E., Ren, H., Rossi, S., Huang, J., 2020b. Wood anatomy of boreal species in a warming world: a review. Iforest 13, 130–138.
Zhang, R., Hu, Z., Cherubini, P., Cooper, D.J., Zhu, L., Lei, P., 2023. Tree-ring data reveal trees are suffering from severe drought stress in the humid subtropical forest. For. Ecol. Manage. 546, 121330.
Zhang, X., Manzanedo, R.D., D'Orangeville, L., Rademacher, T.T., Li, J., Bai, X., Hou, M., Chen, Z., Zou, F., Song, F., Pederson, N., 2019b. Snowmelt and early to mid-growing season water availability augment tree growth during rapid warming in southern Asian boreal forests. Glob. Chang. Biol. 25, 3462–3471.
Zhang, Z., Wu, Q., Hou, M., Tai, B., An, Y., 2021. Permafrost change in Northeast China in the 1950s–2010s. Adv. Clim. Chang. Res. 12, 18–28.

Zhong, Z., He, B., Wang, Y.-P., Chen, H.W., Chen, D., Fu, Y.H., Chen, Y., Guo, L., Deng, Y., Huang, L., Yuan, W., Hao, X., Tang, R., Liu, H., Sun, L., Xie, X., Zhang, Y., 2023. Disentangling the effects of vapor pressure deficit on northern terrestrial vegetation productivity. Sci. Adv. 9, eadf3166.

Zhu, L., Cooper, D.J., Yang, J., Zhang, X., Wang, X., 2018a. Rapid warming induces the contrasting growth of Yezo spruce (*Picea jezoensis* var. *microsperma*) at two elevation gradient sites of northeast China. Dendrochronologia 50, 52–63.

Zhu, L., Wang, X., Neil, P., Chen, Z., Cooper, D.J., Zhang, Y., Li, Z., 2018b. Spatial variability in growth-climate relationships of Amur cork tree (*Phellodendron amurense*) and their connections with PDO in Northeast China. J. Geophys. Res. Biogeo. 123, 1625–1636.

Zhu, L., Yao, Q., Cooper, D.J., Han, S., Wang, X., 2018c. Response of *Pinus sylvestris* var. *mongolica* to water change and drought history reconstruction in the past 260 years, northeast China. Clim. past 14, 1213–1228.

Zhu, L., Cooper, D.J., Han, S., Yang, J., Zhang, Y., Li, Z., Zhao, H., Wang, X., 2021. Influence of the Atlantic multidecadal oscillation on drought in northern Daxing'an Mountains. Northeast China. Catena 198, 105017.

Zhu, L., Zhang, J., Camarero, J.J., Cooper, D.J., Cherubini, P., Yuan, D., Wang, X., 2023. Drivers and spatiotemporal patterns of post-drought growth resilience of four temperate broad-leaved trees. Agric. For. Meteorol. 342, 109741.